JOURNAL OF VIROLOGY, May 2005, p. 6216–6226 Vol. 79, No. 10
0022-538X/05/$08.00+0 doi:10.1128/JVI.79.10.6216–6226.2005

Unusual Topological Arrangement of Structural Motifs in the Baboon Reovirus Fusion-Associated Small Transmembrane Protein

Sandra Dawe,† Jennifer A. Corcoran,‡ Eileen K. Clancy, Jayme Salsman, and Roy Duncan*

Department of Microbiology and Immunology, Dalhousie University, Halifax, Nova Scotia, Canada B3H 4H7

Received 2 November 2004/Accepted 6 January 2005

Select members of the *Reoviridae* are the only nonenveloped viruses known to induce syncytium formation. The fusogenic orthoreoviruses accomplish cell-cell fusion through a distinct class of membrane fusion-inducing proteins referred to as the fusion-associated small transmembrane (FAST) proteins. The p15 membrane fusion protein of baboon reovirus is unique among the FAST proteins in that it contains two hydrophobic regions (H1 and H2) recognized as potential transmembrane (TM) domains, suggesting a polytopic topology. However, detailed topological analysis of p15 indicated only the H1 domain is membrane spanning. In the absence of an N-terminal signal peptide, the H1 TM domain serves as a reverse signal-anchor to direct p15 membrane insertion and a bitopic $N_{exoplasmic}/C_{cytoplasmic}$ topology. This topology results in the translocation of the smallest ectodomain (~20 residues) of any known viral fusion protein, with the majority of p15 positioned on the cytosolic side of the membrane. Mutagenic analysis indicated the unusual presence of an N-terminal myristic acid on the small p15 ectodomain is essential to the fusion process. Furthermore, the only other hydrophobic region (H2) present in p15, aside from the TM domain, is located within the endodomain. Consequently, the p15 ectodomain is devoid of a fusion peptide motif, a hallmark feature of membrane fusion proteins. The exceedingly small, myristoylated ectodomain and the unusual topological distribution of structural motifs in this nonenveloped virus membrane fusion protein necessitate alternate models of protein-mediated membrane fusion.

The baboon reovirus (BRV) p15 protein is a novel member of the recently described fusion-associated small transmembrane (FAST) protein family (9, 11, 45). The FAST proteins are unusual membrane fusion proteins encoded by the fusogenic subgroup of orthoreoviruses, one of the few examples of nonenveloped viruses that induce cell-cell fusion and syncytium formation (15, 18). At 10 to 15 kDa, the reovirus FAST proteins are the smallest known viral membrane fusion proteins and are unlikely to undergo the types of extensive structural rearrangements required for enveloped virus fusion protein activity (27, 48). The FAST proteins are also the only examples of nonstructural viral proteins that induce membrane fusion (11, 45). As a result of their nonstructural nature, the FAST proteins play no role in reovirus entry. Their sole purpose appears to reflect enhanced dissemination of the infection via syncytium formation, following FAST protein expression in reovirus-infected cells (16, 17). The unusual structural features of the FAST proteins and their unique role in the virus replication cycle suggest the mechanism of FAST-mediated membrane fusion is unlikely to adhere to the existing paradigm, which is derived from studies of the enveloped virus fusion proteins (5, 48, 52).

In addition to BRV p15, FAST proteins have been recently characterized from avian reovirus (ARV), Nelson Bay reovirus (NBV), and reptilian reovirus (RRV) (9, 45). Although there is no significant amino acid sequence identity between the different FAST proteins, they do share several common biophysical features: all are small, acylated, integral membrane proteins containing a membrane-proximal cluster of polybasic residues (9, 11, 46). There are, however, more differences than similarities between the FAST proteins, in both their repertoire and arrangement of structural motifs. For example, the RRV p14 and BRV p15 FAST proteins contain no essential cysteine residues and therefore lack two of the defining p10 structural motifs, a predicted ectodomain cystine noose and the palmitoylated dicysteine motif in the endodomain, both of which are required for p10 fusion activity (46, 47). Furthermore, while p10 is palmitoylated, both p14 and p15 are N-terminally myristoylated (9, 11), and p14 and p15 each contain a polyproline motif (PPXPPP) that is absent from p10, although this motif is C proximal in p14 and N proximal in p15 (9, 11). The diversity in arrangement and repertoire of structural motifs and (by inference) protein structure in this presumably related family of membrane fusion proteins is quite remarkable. Assuming the FAST proteins evolved from a common progenitor, it would appear that the mechanism of membrane fusion has placed few constraints on their evolution. The structural diversity of the FAST proteins suggests that FAST-mediated membrane fusion may not be dependent on the types of precise protein conformational changes and lipid rearrangements that occur during membrane fusion mediated by enveloped virus fusion proteins.

Topological analysis indicates p10 and p14 are bitopic membrane proteins with N-terminal exoplasmic and C-terminal cytoplasmic domains (N_{exo}/C_{cyt}) (9, 45). These proteins use their

* Corresponding author. Mailing address: Department of Microbiology and Immunology, Faculty of Medicine, Dalhousie University, Halifax, Nova Scotia, Canada B3H 1X5. Phone: (902) 494-6770. Fax: (902) 494-5125. E-mail: roy.duncan@dal.ca.

† Present address: McArdle Laboratory for Cancer Research, University of Wisconsin, Madison, WI 53706.

‡ Present address: Department of Medical Microbiology and Immunology, Heritage Medical Research Building, University of Alberta, Edmonton, Alberta, Canada T6G 2S2.

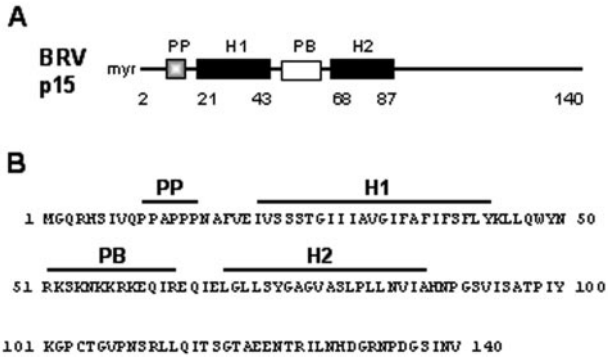

FIG. 1. BRV p15 structural motifs. (A) Representation of p15 indicating the N-terminal myristate moiety (myr), the polyproline motif (PP), the two hydrophobic motifs (H1 and H2), and the polybasic motif (PB). Numbers refer to residue positions. (B) Sequence of the BRV p15 protein. The residues corresponding to the motifs presented in panel A are overlined.

transmembrane (TM) domains as reverse signal-anchors to direct translocation of the N terminus across the membrane. This topology results in small ectodomains of approximately 40 residues and places a membrane-proximal, polybasic region within their 40- to 70-residue endodomains, consistent with the "positive-inside rule" of membrane protein topology (26). Within their ectodomains, p10 and p14 each contain a moderately hydrophobic region of 14 to 16 residues that may serve as a fusion peptide (10, 47), in a manner analogous to the fusion peptides of enveloped viruses (19, 28, 49). The N_{exo}/C_{cyt} topology also indicates that the essential palmitoylated dicysteine motif of p10 influences p10 syncytium formation from a cytosolic location (46). In contrast, p14 is a rare example of an integral membrane protein that translocates an N-terminal myristate moiety across the membrane bilayer; therefore, the fatty acid must exert its influence on p14 membrane fusion activity from an exoplasmic location (9).

Relatively little is known about the BRV p15 FAST protein, and its topology in the membrane has not been determined. Sequence analysis indicates p15 contains no N-terminal cleavable signal peptide to direct protein topology in the membrane (11). Numerous topology-predicting algorithms identified two hydrophobic motifs (H1, residues 21 to 43; H2, residues 68 to 87) as potential TM domains (Fig. 1), suggesting that p15 utilizes these motifs as signal-anchor sequences to direct a polytopic membrane topology. However, these algorithms disagree as to the predicted topology of the protein. Since positive residues adjacent to a TM domain are generally retained in the cytosol (3, 26), the presence of the p15 polybasic region between H1 and H2 favors a N_{exo}/C_{exo} polytopic topology for p15. However, the myristate moiety in the vast majority of myristoylated proteins interacts with the cytosolic leaflet of the plasma membrane (42); therefore, the presence of an N-terminal myristate in p15 (11) suggests an N_{cyt} topology.

The uncertainty pertaining to p15 membrane topology precludes any meaningful assessment of the possible roles of key structural motifs. For instance, if both H1 and H2 serve as TM domains, then p15 is devoid of a fusion peptide motif, since there are no other clusters of apolar amino acids in p15 that could serve a similar function. Similarly, it has not been determined whether the myristoylated N terminus of p15 influences p15 topogenesis or fusion activity and if so, whether this fatty acid exerts its influence from the endoplasmic or exoplasmic side of the membrane.

Following a detailed topological analysis of p15, we now report that p15 is a type III membrane protein, adopting an N_{exo}/C_{cyt} topology and utilizing the H1 region as a reverse signal-anchor sequence to direct membrane insertion and topology. This surprising plasma membrane topology localizes both the N-terminal myristate moiety (which we show is required for fusion activity) and a polyproline motif to a remarkably small, 20-residue ectodomain. More importantly, this topology places the second hydrophobic motif in the cytosol, leading to the absence of a hydrophobic fusion peptide motif in the p15 ectodomain.

MATERIALS AND METHODS

Cells and antibodies. For ease of transfection, quail fibroblast (QM5) cells (which are permissive for BRV infection) were used to express p15 constructs. QM5 cells (16) were maintained at 37°C in a 5% CO_2 atmosphere, grown in medium 199 with Earle's salts containing 10% heat-inactivated fetal bovine serum (FBS) and 100 U of penicillin and streptomycin per ml. To generate p15-specific antisera, a recombinant baculovirus expressing p15 under the control of the polyhedrin promoter was created using the Bac-To-Bac Baculovirus Cloning and Expression system (Life Technologies). The p15 protein was purified from infected SF21 cells by detergent disruption, affinity chromatography using TALON Metal Affinity Resin (Clonetech), and ion-exchange chromatography using HiTrap SP HP ion-exchange columns (Amersham Pharmacia Biotech). The purified p15 (500 μg per injection) was used to immunize rabbits with Freund's complete adjuvant for the primary injection and Freund's incomplete adjuvant for five subsequent booster injections at 6-week intervals. The polyclonal antiserum specific for the C terminus of p15 (residues 90 to 140) was previously described (11).

Cloning. Site-directed mutagenesis was used to create numerous alterations in the p15 N-terminal, polybasic, and C-terminal regions for topological and functional analyses. The Stratagene Quick-Change mutagenesis method was used according to the manufacturer's specifications to eliminate the p15 myristoylation consensus sequence (G2A construct). The Stratagene Excite mutagenesis method was used to (i) insert a double-hemagglutinin (HA) antigenic epitope tag [(YPYDVPDYA)×2] into the p15 N-terminal domain after amino acid 8 (HAN construct), into the polybasic region following residue 59 (HAB construct), or into the C-terminal domain following residue 140 (HAC construct); (ii) insert the protein kinase A (PKA) consensus sequence (LRRASLG) into authentic p15, following the amino acid residues indicated by the name of the construct (constructs 8pka, 59pka, and 140pka) or into the various substituted construct backbones described above (constructs G2A-8pka, G2A-59pka, and G2A-140pka); and (iii) exchange the TM domain of the p14 FAST protein with the H1 region of p15 (14TM15 construct). Authentic p15 and the G2A construct were also each cloned in frame with green fluorescent protein (GFP), separated by a six-glycine spacer, using the HindIII and BamHI restriction sites of the pEGFP-N1 vector (Clontech). The sequence of all constructs was confirmed by cycle sequencing using the Thermo Sequenase Radiolabeled Terminator Cycle Sequencing kit (United States Biochemical) according to the manufacturer's instructions.

Radiolabeled cell lysates. QM5 cells seeded in six-well dishes were transfected with Lipofectamine (Life Technologies) and 1 μg of DNA in serum-free medium. The transfection mixture was replaced after 4 h with medium containing 10% FBS. To generate [^{3}H]leucine-labeled lysates, cells were leucine starved for 15 min and then radiolabeled for 45 min with 50 μCi of [^{3}H]leucine (Amersham Biosciences) per ml of leucine-free medium, prepared from the MEM Select-Amine kit (Life Technologies). Alternatively, transfected monolayers were labeled for 4 h with 20 μCi of [^{3}H]myristate (Amersham Biosciences) per ml of Eagle's minimal essential medium (MEM; Life Technologies) containing 1% dialyzed FBS. To generate ^{32}P-labeled lysates, cells were incubated 40 min with phosphate-free Dulbecco's MEM (Sigma) in the presence or absence of 100-μg/ml cycloheximide and then labeled with 100 μCi of [^{32}P]orthophosphate (Amersham Biosciences) per ml of phosphate-free Dulbecco's MEM containing 20 μM forskolin in the presence or absence of 100-μg/ml cycloheximide. Radiolabeled monolayers were then rinsed three times with phosphate-buffered saline (140 mM NaCl, 2.5 mM KCl, 10 mM Na_2HPO_4, and 2 mM KH_2PO_4) and lysed

in cold RIPA buffer (50 mM Tris-HCl [pH 8], 150 mM NaCl, 1 mM EDTA, 1% Igepal, 0.5% sodium deoxycholate, and 0.1% sodium dodecyl sulfate [SDS]) containing protease inhibitors (200 nM aprotinin, 1 μM leupeptin, and 1 μM pepstatin; Sigma) and phosphatase inhibitors (500 μM nitrophenyl phosphate, 50 μM sodium orthovanadate, 1 mM sodium fluoride, and 1 mM EDTA; Sigma), as required. Cell lysates were harvested, and the nuclei were pelleted for 1 min at 10,000 × *g* in a bench-top microfuge. Immune precipitations of radiolabeled lysates using anti-p15 antisera and analysis of samples by fluorography and SDS–15% polyacrylamide gel electrophoresis (PAGE) were described previously (11).

In vitro transcription, translation, and membrane fractionation. BRV p15 mRNA was transcribed and translated in vitro as previously described (11), using T7 RNA polymerase and rabbit reticulocyte lysates in the presence or absence of microsomal membranes (Promega). The membrane-containing fraction of translation reactions was collected after centrifugation for 30 min at 10,000 × *g* in a bench-top microfuge at 4°C. To remove peripherally associated membrane proteins, the membrane pellet was treated with either high salt (500 mM NaCl) or high pH (100 mM Na_2CO_3, pH 11.5) on ice for 30 min and then recentrifuged. [^{3}H]leucine-labeled p15 was analyzed by fluorography and SDS–15% PAGE.

Nuclei staining and syncytial indexing. QM5 cells grown in 12-well plates were transfected as above. Monolayers were fixed, permeabilized with methanol, and stained with Wright-Giemsa stain (Diff-Quik) according to the manufacturer's instructions (VWR Scientific) to visualize cell nuclei and polykaryon formation. In some experiments, cells were incubated in the presence of brefeldin A (1 μg/ml) to inhibit endoplasmic reticulum (ER)-Golgi transport. The inhibitor was added to cells approximately 12 to 15 h posttransfection, just prior to the onset of syncytium formation, and cells were incubated for an additional 3 h prior to fixation and staining. The relative ability of various p15 constructs to mediate syncytium formation was determined by light microscopy at magnification of ×200.

Immunostaining. Transfected monolayers were methanol fixed 20 to 27 h posttransfection, prior to immunostaining. Monolayers were preblocked with phosphate-buffered saline containing 25-μg/ml whole goat immunoglobulin G (IgG) (Jackson ImmunoResearch), and transfected foci were detected with primary rabbit polyclonal antiserum specific for p15 (diluted 1:800 to 1:1,000). Foci were visualized with secondary goat anti-rabbit F(ab′)$_2$ conjugated to either alkaline phosphatase (Jackson ImmunoResearch, diluted 1:1,000), fluorescein isothiocyanate (FITC; Jackson ImmunoResearch, diluted 1:800), or Alexa 555 (Molecular Probes, diluted 1:800). For coimmunofluorescence, monolayers were additionally stained using mouse anti-calnexin antibody (BD Transduction Laboratories, diluted 1:1,000) and tetramethyl rhodamine isothiocyanate-conjugated goat anti-mouse IgG (Jackson ImmunoResearch, diluted 1:1,000). The specificity of the antibody staining was confirmed using normal rabbit serum with conjugated secondary antibodies to stain p15-transfected cells or the p15 polyclonal antiserum and secondary antibodies to stain mock-transfected cells. Both controls gave minimal background staining under the stated conditions. Cells fixed on coverslips and stained for immunofluorescence were mounted on glass slides with fluorescent mounting medium (Dako). Images of immunocytochemically stained cells were captured using a Nikon Diaphot inverted microscope (magnification, ×200) and computer software Image-Pro Plus (version 4.0). Images of immunofluorescently stained cells were captured using either a Ziess Axiovert microscope (magnification, ×630) and Axiovision software or a Zeiss LSM510 scanning argon laser confocal microscope.

Visualization of plasma membrane-localized p15. To detect cell surface-expressed p15, cells seeded on coverslips in cluster plates were transfected as above when subconfluent (to ease visualization of single-cell foci). The intracellular pool of p15 was depleted prior to immunofluorescent staining by treatment with cycloheximide for 1 to 3 h (100 μg/ml) at 18 to 20 h posttransfection. Monolayers were then methanol fixed and immunostained as described above. Indirectly stained immunofluorescent p15-transfected cells, as well as GFP- and GFP-chimera-transfected cells, were visualized and photographed with a Zeiss LSM510 scanning argon laser confocal microscope. Images shown represent one *Z* section (approximately 0.1 μM).

Cell-surface fluorescence microscopy. QM5 cells were seeded on coverslips and transfected with the HA-tagged p15 constructs (HAN, HAB, or HAC) at 80% confluency with Lipofectamine 2000 (Invitrogen). At 27 h posttransfection, cells were either fixed and permeabilized with methanol for staining of intracellular HA-tagged p15 or washed with Hank's balanced salt solution and placed on ice for staining of surface-localized HA epitopes. Both permeabilized and nonpermeabilized cells were blocked with whole goat IgG (1:1,000) for 30 min and then stained with mouse monoclonal anti-HA (1:200 for surface staining; 1:400 for intracellular staining) for 1 h. Cells were washed three times in succession with Hank's balanced salt solution and then three times for 10 min each before incubation with goat anti-mouse secondary antibody (1:200 for surface staining; 1:400 for intracellular staining) conjugated to Alexa 555 (Molecular Probes) for 1 h. Washing was performed as above, and nonpermeabilized cells were subsequently fixed with methanol before the coverslips were mounted on slides using fluorescent mounting medium (Dako). Stained cells were visualized and photographed with the 100× objective of a Zeiss LSM510 scanning neon laser confocal microscope.

RESULTS

BRV p15 traffics through the ER-Golgi pathway to the plasma membrane. In a recent publication describing the identification of p15, this novel FAST protein was shown to be a nonstructural, integral membrane protein (11). Sequence analysis also identified a functional N-terminal myristoylation site, an N-proximal polyproline motif, and two hydrophobic motifs (H1 and H2) separated by a polybasic region (Fig. 1). The trafficking, subcellular localization, and membrane topology of p15 have not been described. As a first step in further characterization of p15, transfected cells were treated with brefeldin A to inhibit the ER-Golgi transport pathway (38). As indicated (Fig. 2A), brefeldin A treatment prevented p15-induced syncytium formation, suggesting a role for ER-Golgi trafficking in p15-induced syncytium formation. Immunofluorescent staining was also used to assess p15 subcellular localization. Staining of permeabilized, p15-transfected cells with polyclonal anti-p15 antiserum revealed strong perinuclear staining and a punctate, reticular staining pattern extending throughout the cytosol (Fig. 2B). In addition, a significant level of cofluorescence was observed in transfected cells stained for both p15 and the ER marker calnexin, suggesting that p15 is targeted to the ER. The intracellular fluorescence of p15 obscured clear visualization of any plasma membrane-localized p15. Therefore, translation was inhibited by treatment for 1 to 3 h with cycloheximide to deplete the intracellular p15 pools and allow transport of preexisting p15 to the plasma membrane. Under these conditions, clear ring fluorescence was observed at the plasma membrane, following antibody staining of permeabilized cells with anti-p15 antiserum (Fig. 3). The specificity of the immunostaining was confirmed by the absence of staining using normal rabbit serum (Fig. 3c and d), and by the lack of staining of cells not expressing p15 in the transfected monolayers (Fig. 2A and B). The latter point was confirmed by the absence of specific staining of mock-transfected cells by the p15 antiserum (data not shown). Based on the immunofluorescent staining patterns and the results obtained with brefeldin A, we infer that newly synthesized p15 is targeted to the ER and at least a proportion of p15 traffics through the cell secretory pathway to the plasma membrane.

Epitope-tagging of p15 suggests a bitopic N_{exo}/C_{cyt} topology. Polyclonal antisera raised against either the full-length, baculovirus-expressed p15 or the C-terminal domain (residues 90 to 140) expressed as a maltose binding protein-p15 chimera in *Escherichia coli* exhibited no detectable reaction with the surface of p15-transfected cells, as determined by a syncytium inhibition assay or cell-surface immunofluorescent staining (data not shown). Therefore, to determine the topology of p15 in the plasma membrane, we inserted double-HA epitope tags into the N-terminal, C-terminal, or polybasic regions. The N-terminal epitope tags (p15-HAN construct) were inserted after residue 8, between the N-terminal myristoylation consensus

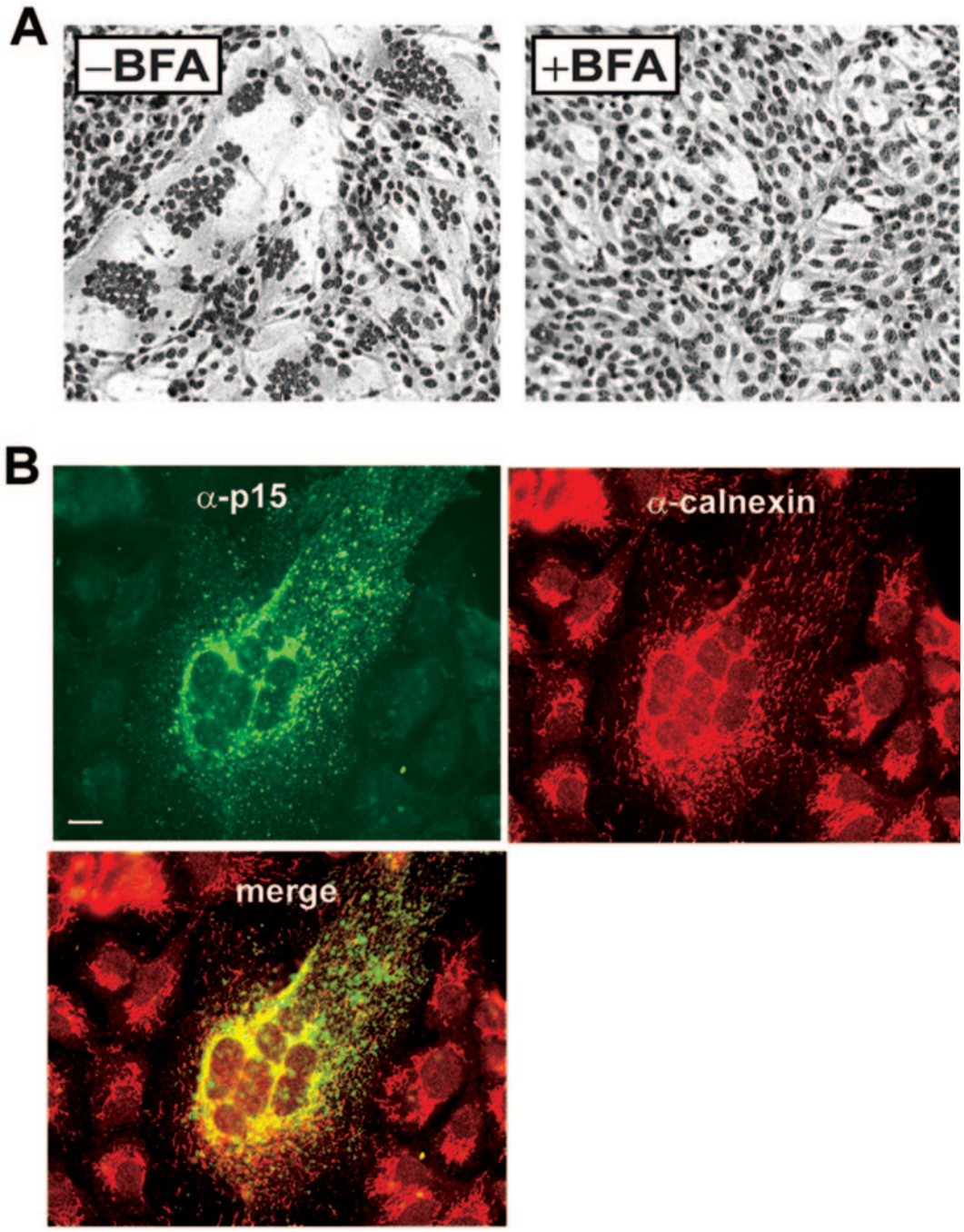

FIG. 2. BRV p15 is targeted to the endoplasmic reticulum. (A) Transfected cells expressing p15 were incubated in the absence or presence of brefeldin A, as outlined in Materials and Methods. The extent of syncytium formation was determined by Wright-Giemsa staining to reveal the presence of clustered nuclei in polykaryons, and images were captured by light microscopy at ×170 magnification. (B) Transfected cells expressing p15 were methanol-fixed and coimmunostained using rabbit anti-p15 polyclonal antiserum and FITC-conjugated goat anti-rabbit F(ab′)2 (α-p15 panel), followed by mouse anti-calnexin and rhodamine-conjugated goat anti-mouse IgG (α-calnexin panel). The bottom panel shows a merge of the images in the first two panels, with colocalization indicated by the yellow color. Scale bar, 10 μm.

sequence and the polyproline motif (Fig. 1). This epitope tag did not adversely affect p15 myristoylation (data not shown). The p15-HAB construct contained the double-epitope tag inserted after residue 59 in the polybasic region, which lies between the two hydrophobic motifs, while the p15-HAC construct was tagged at the extreme C terminus of p15 by in-frame insertion after residue 140. Both the p15-HAN and p15-HAB constructs were nonfusogenic, while the p15-HAC construct retained full fusion activity (data not shown).

Transfected cells expressing these three constructs were stained with anti-HA monoclonal antibodies, either without permeabilization to detect surface-exposed epitopes or follow-

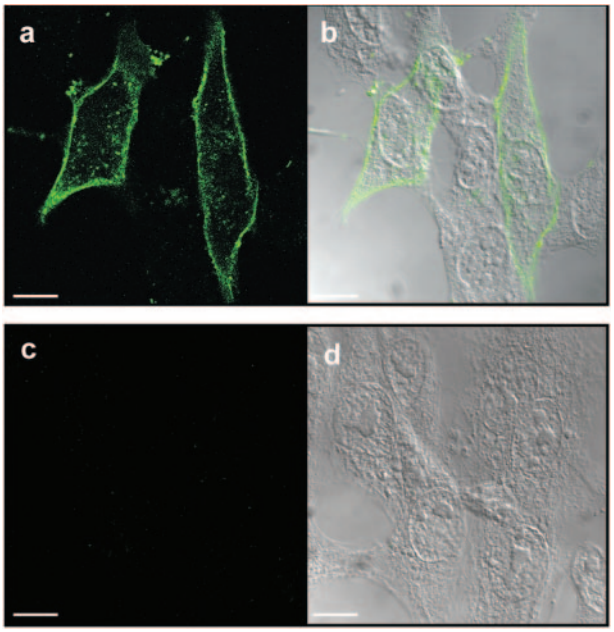

FIG. 3. BRV p15 is trafficked to the plasma membrane. BRV p15-transfected cells were treated (20 h posttransfection) for 1 h with cycloheximide prior to methanol-fixation and immunostaining using p15-specific rabbit antiserum (a and b), or normal rabbit serum (c and d), and FITC-conjugated secondary goat anti-rabbit F(ab′)2. Cell images were captured by confocal microscopy. Left panels are fluorescent images, while the right panels are an overlay of the fluorescent image and the differential interference contrast (DIC) microscopy image. Scale bar, 10 μm.

ing fixation and permeabilization to reveal the intracellular distribution of the tagged p15 (Fig. 4). Fluorescent staining of permeabilized cells revealed all three proteins were expressed in transfected cells and displayed the broadly distributed, punctate intracellular staining pattern characteristic of authentic p15 (Fig. 4B, top panels). Immunostaining of unfixed, nonpermeabilized cells expressing the p15-HAN construct clearly revealed surface exposure of the epitope tag at the periphery of transfected cells (Fig. 4B, panel d). In contrast, staining nonpermeabilized cells expressing the p15-HAB or p15-HAC constructs (Fig. 4B, panels e and f, respectively) failed to detect any specific fluorescence. The inability to detect surface expression of the HAC tag was not due to a failure of this construct to traffic to the plasma membrane since p15-HAC retained the full cell-cell fusion activity of authentic p15 (data not shown) implying plasma membrane localization in the correct topology. Similarly, immunofluorescent staining of permeabilized cells treated with cycloheximide detected p15-HAC and the two nonfusogenic constructs (HAN and HAB) at the periphery of transfected cells (Fig. 4B, panels g to i) suggesting plasma membrane localization. These results implied that p15 assumes a bitopic membrane topology with an N-terminal ectodomain, retaining both the polybasic region and the C-terminal domain in the cytosol.

Phosphorylation analysis indicates the polybasic and C-terminal domains of p15 are cytosolic. To obtain direct evidence for the cytosolic localization of the polybasic region and C-terminal domain of p15, and to confirm the N-out bitopic topology predicted using the HA epitope-tagging procedure, we used in vivo phosphorylation analysis. Goder et al. (24) demonstrated the value of site-specific phosphorylation by PKA as a sensor of cytosolic localization to determine protein topology. The consensus sequence (LRRASLG) for serine-phosphorylation by PKA (designated here as a pka tag) was inserted into the N-terminal, polybasic, or C-terminal regions of p15 (after residues 8, 59, and 140, respectively) (Fig. 5A). As with the HA epitope tags, insertion of the pka tag into the N-terminal domain eliminated p15 fusion activity while addition of the tag to the C terminus of p15 (140pka construct) had no deleterious effect on p15 fusion activity (data not shown). Insertion of the 7-residue pka tag into the polybasic region did not have the same adverse effect as insertion of the 18-residue double-HA tag; the p15-to-59pka construct displayed robust fusion activity, fusing monolayers to completion at approximately 70% of the rate of authentic p15 (data not shown). [^{3}H]leucine labeling revealed the various constructs were expressed at comparable levels (Fig. 5B, lanes 1 to 4). Radiolabeling with [^{32}P]orthophosphate in the presence of 20 μM forskolin, an indirect activator of PKA, did not label authentic p15, indicating the absence of cryptic phosphorylation signals in the protein (Fig. 5B, lane 5). Insertion of the pka tag into the polybasic or C-terminal regions of p15 led to efficient phosphate radiolabeling (Fig. 5B, lanes 7 and 8), implying that both regions are localized in the cytosol. In contrast, the N-proximal tag exhibited a very low, but detectable, level of phosphorylation (Fig. 5B, lane 6).

Since there is no cleavable N-terminal signal sequence in p15, the TM domain must serve as a signal-anchor sequence to direct p15 insertion into the membrane (51). Consequently, the low level of phosphorylation of the N-proximal pka tag could have resulted from transient exposure of the N terminus of p15 to cytosolic PKA, prior to emergence of the internal signal-anchor from the ribosome and targeting of the nascent p15 to the ER translocon. Such cotranslational phosphorylation of a pka tag present in a small N-terminal ectodomain has been previously reported (24). To test this hypothesis, phosphate incorporation into the various constructs was analyzed after cycloheximide treatment to stop protein synthesis, following a brief chase period to allow membrane insertion of the preexisting p15 proteins. Incubation with cycloheximide completely blocked translation, as evidenced by the absence of [^{3}H]leucine incorporation into host cell proteins (Fig. 5B, lanes 9 and 10). The p15 proteins tagged in the polybasic or C-terminal regions were still phosphorylated in the presence of cycloheximide (Fig. 5B, lanes 13 and 14). In contrast, cycloheximide treatment completely abolished labeling of the N-terminally tagged construct (Fig. 5B, lane 12), indicating that the limited phosphorylation of this construct observed without cycloheximide occurred cotranslationally. Similar results were obtained using cycloheximide and the pka tag approach to analyze the topology of the H1 subunit of the asialylyglycoprotein receptor (24).

Based on the results obtained from both immunofluorescent staining and site-specific phosphorylation, we propose that p15 assumes a bitopic N_{exo}/C_{cyt} topology retaining both the C-terminal and polybasic regions of p15 in the cytosol.

The H1 region functions as a signal-anchor. The topological analysis predicted the p15 H1 region serves as a reverse signal-anchor to direct the unique N_{exo}/C_{cyt} membrane topology. To

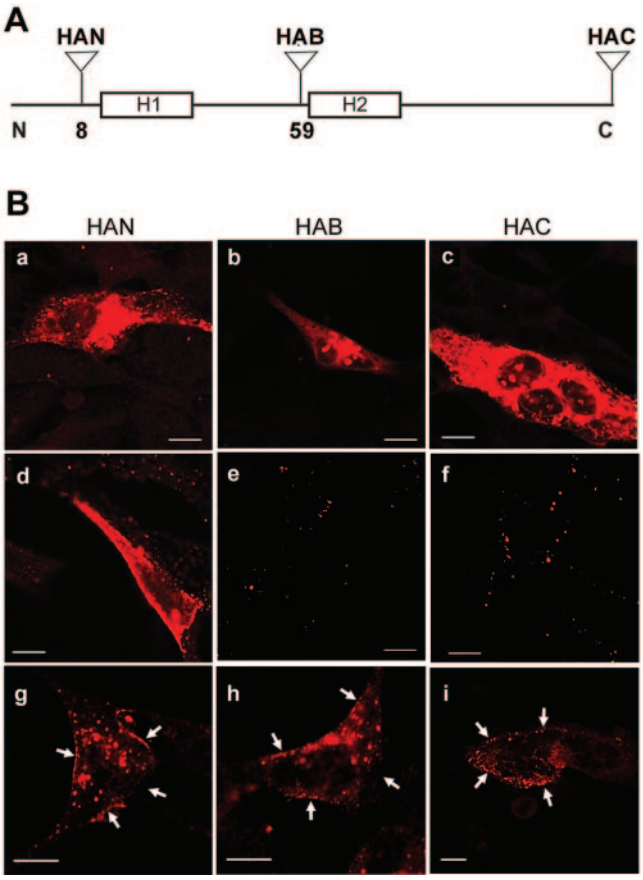

FIG. 4. Surface immunofluorescence with epitope-tagged p15. (A) Schematic diagram indicating the locations of insertion of double-HA epitope tags into the N-terminal (HAN), polybasic (HAB), and C-terminal (HAC) domains. The tags were inserted after the indicated residue. In the case of HAC, the tag was inserted in frame after the last residue of p15. The two hydrophobic domains (H1 and H2) are indicated. (B) Cells were transfected with p15 constructs carrying HA epitope tags in the N-terminal (HAN), polybasic (HAB), or C-terminal (HAC) regions. At 24 h posttransfection, cells were fixed and permeabilized with methanol for staining of intracellular HA-tagged p15, either without (a to c) or after (g to i) treatment of cells with cycloheximide, or chilled and left unfixed for staining of surface-localized HA epitopes (d to f). Cells were stained with either mouse monoclonal anti-HA (a to f) or rabbit anti-p15 (g to i), and the appropriate secondary antibody was conjugated to Alexa 555. Stained cells were visualized and photographed using confocal microscopy. The arrows (g to i) indicate the edges of the cell as observed under DIC microscopy. Scale bars, 10 μm.

provide additional evidence for this prediction, the H1 region of p15 was used to replace the single TM domain of the p14 FAST protein that serves as a reverse signal-anchor to direct the functional N_{exo}/C_{cyt} membrane topology of p14 (9). The first charged residues flanking either end of these hydrophobic regions were used to define the boundaries of each TM domain (in each case, a glutamic acid residue flanked the N terminus and a lysine residue flanked the C terminus; Fig. 6A). Creation of this chimeric 14TM15 construct resulted in replacement of the 19-residue TM domain of p14 with 23 residues of the H1 region of p15. The authentic and chimeric p14 proteins were expressed in transfected cells and observed for syncytium formation as an indicator of p14 expression in the correct, functional membrane topology. As shown (Fig. 6B), the 14TM15 construct was highly fusogenic, fusing monolayers to completion, although the fusion kinetics were delayed by approximately 4 h relative to authentic p14. Therefore, the p15 H1 region can serve as an effective reverse signal-anchor to direct the N_{exo}/C_{cyt} topology of a heterologous protein.

N-terminal myristoylation is essential to p15-induced membrane fusion. Previous results indicated p15 is myristoylated at its N terminus (11). The predicted N_{exo}/C_{cyt} topology, therefore, would place the myristate moiety external to the plasma membrane. To investigate the role, if any, of N-myristoylation in the topogenesis and/or fusion activity of p15, a G2A substitution was inserted into p15, thereby removing the penultimate, myristate-accepting glycine residue. While both authentic p15 and the G2A mutant were labeled with [^{3}H]leucine, only authentic p15 incorporated [^{3}H]myristate (Fig. 7A). The nonmyristoylated G2A construct interacted with membranes in a manner indistinguishable from that of authentic p15, behaving as an integral membrane protein (Fig. 7B), and assuming the correct N_{exo}/C_{cyt} topology as determined by phosphate radiolabeling of the pka-tagged versions of the G2A p15 protein (Fig. 7C). The myristate moiety, therefore, plays no significant role in determining the N_{exo}/C_{cyt} topology of p15. Myristoylation is, however, essential for the fusion activity of p15. When expressed in transfected cells, the G2A construct failed to induce cell-cell fusion and syncytium formation (Fig. 7D). The loss of fusion activity did not appear to reflect gross changes in p15 subcellular localization, since GFP-tagged G2A displayed the same plasma membrane-localization pattern as GFP-tagged authentic p15 (Fig. 8). Thus, a myristoylated ectodomain does not influence p15 membrane association, topology, or surface expression, but is essential for p15-induced syncytium formation.

DISCUSSION

Topological analysis of p15. A previous publication reported that p15, like the other FAST proteins, is a small, acylated, integral membrane protein (9, 11, 45). Based on the presence of two potential TM domains, we speculated that p15 might assume a polytopic membrane topology (11). We now show that p15 spans the membrane just once, utilizing the H1 region (residues 21 to 43) as an internal reverse signal-anchor sequence to direct an N_{exo}/C_{cyt} membrane topology. This topology results in an unusual distribution of the p15 structural motifs (Fig. 9).

Analysis of surface immunofluorescence using HA-tagged p15 constructs (Fig. 4) provided direct evidence that the N-terminal domain of p15 resides outside the cell, and indirect evidence that the polybasic and C-terminal regions are localized to the cytosol. Further indirect support that the C terminus of p15 represents the endodomain was provided by the inability of a high-titer polyclonal antisera specific for the C-terminal 50 residues of p15 to detect surface expression of this domain, using either a syncytial inhibition assay or surface immunofluorescent staining (data not shown). Direct evidence that the p15 polybasic region and C-terminal domain are retained in the cytoplasm was obtained by demonstrating that both regions were efficiently phosphorylated posttranslationally. The HA epitope-tagging and phosphorylation analyses

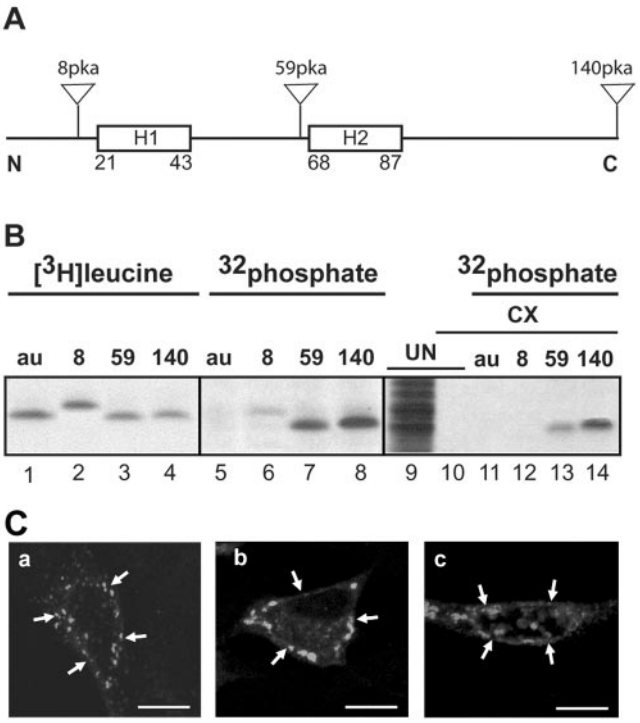

FIG. 5. Phosphorylation mapping indicates the p15 H1 region serves as an internal reverse signal anchor to direct a bitopic N_{exo}/C_{cyt} topology. (A) Schematic diagram indicating the relative positions within p15 of introduced sites for phosphorylation by PKA (8pka, 59pka, and 140pka). The two hydrophobic domains (H1 and H2) are indicated with the numbers reflecting residue positions. (B) Transfected cells expressing authentic p15 (au) and the p15 constructs tagged with the PKA consensus sequence after residue 8, 59, or 140 were radiolabeled with [^{3}H]leucine (lanes 1 to 4, 9, and 10) or [^{32}P]phosphate (lanes 5 to 8 and 11 to 14); CX indicates the presence of cycloheximide prior to and during radiolabeling. Cell lysates were immune precipitated with anti-p15 antiserum, separated by SDS–15% PAGE, and detected by fluorography. UN, untransfected cells radiolabeled with [^{3}H]leucine without (lane 9) or with (lane 10) cycloheximide treatment and analyzed without immune precipitation. (C) Transfected cells expressing the 8pka (a), 59pka (b), or 140pka (c) p15 constructs were treated with cycloheximide for 3 h prior to methanol fixation at 27 h posttransfection. Cells were stained with rabbit anti-p15 and the appropriate secondary antibody conjugated to Alexa 555. Stained cells were visualized and photographed by confocal microscopy. The arrows indicate the edges of the cell as observed under DIC microscopy. Scale bars, 10 μm.

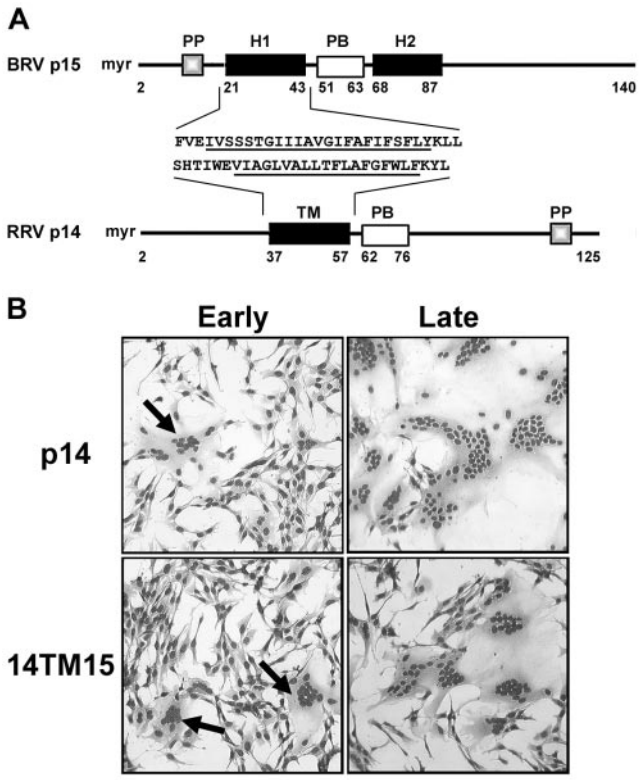

FIG. 6. The p15 H1 domain functions as a reverse signal-anchor to direct the N_{exo}/C_{cyt} topology of a heterologous protein. (A) The linear arrangement of structural motifs in the BRV p15 and RRV p14 FAST proteins are depicted. The N-terminal myristate moieties (myr), the polyproline motifs (PP), the polybasic motifs (PB), the two p15 hydrophobic motifs (H1 and H2), and the p14 TM domain are indicated. Numbers refer to residue positions. The sequences in the region of the p15 H1 domain and p14 TM domain are indicated. Underlined sequences indicate the presumed signal-anchor sequences and the sequences that were exchanged to substitute the p15 H1 domain for the p14 TM domain in the 14TM15 construct. (B) Transfected cells expressing authentic p14 or the 14TM15 construct were fixed and Wright-Giemsa stained at early (4.5 or 8.5 h for p14 and 14TM15, respectively) and late (8.5 or 13.5 h for p14 and 14TM15, respectively) times posttransfection to reveal the extent of syncytium formation. Both constructs induced efficient syncytium formation. Arrows in the left hand panels indicate the presence of small syncytia at the early time points.

both predicted that the H1 hydrophobic region of p15 serves as a reverse signal-anchor sequence to direct p15 membrane insertion in a unique N_{exo}/C_{cyt} topology. This prediction was further confirmed by demonstrating that H1 can effectively substitute for the single TM domain in the RRV p14 protein to direct the functional N_{exo}/C_{cyt} topology of this related FAST protein (Fig. 6).

We noted that the pka tag in the polybasic region was consistently radiolabeled slightly less efficiently than the tag incorporated at the extreme C terminus of p15, both with authentic p15 and with the nonmyristoylated p15-G2A construct (Fig. 5 and 7). This was not due to transient cotranslational cytosolic exposure of the polybasic region, as occurs with the N-terminal domain, since the same relative degree of phosphorylation of 59pka occurred posttranslationally when cells were treated with cycloheximide (Fig. 5). In addition, labeling of 59pka, while reduced relative to 140pka, far exceeded the limited cotranslational labeling of the 8pka construct (Fig. 5). It seems likely that the short distance separating the polybasic pka tag from the membrane (16 residues from the predicted C terminus of H1) and/or interaction of this highly charged region with anionic phospholipid headgroups or with other regions of the protein rendered it slightly less accessible to PKA. An alternate explanation is that p15 can assume two different bitopic topologies using either H1 or H2 as a TM domain, with the latter topology resulting in translocation of the polybasic region across the membrane and reduced phosphorylation. Although we cannot formally exclude this possibility, such a topology would require the unlikely translocation across the membrane of both a functional TM domain (the H1 region)

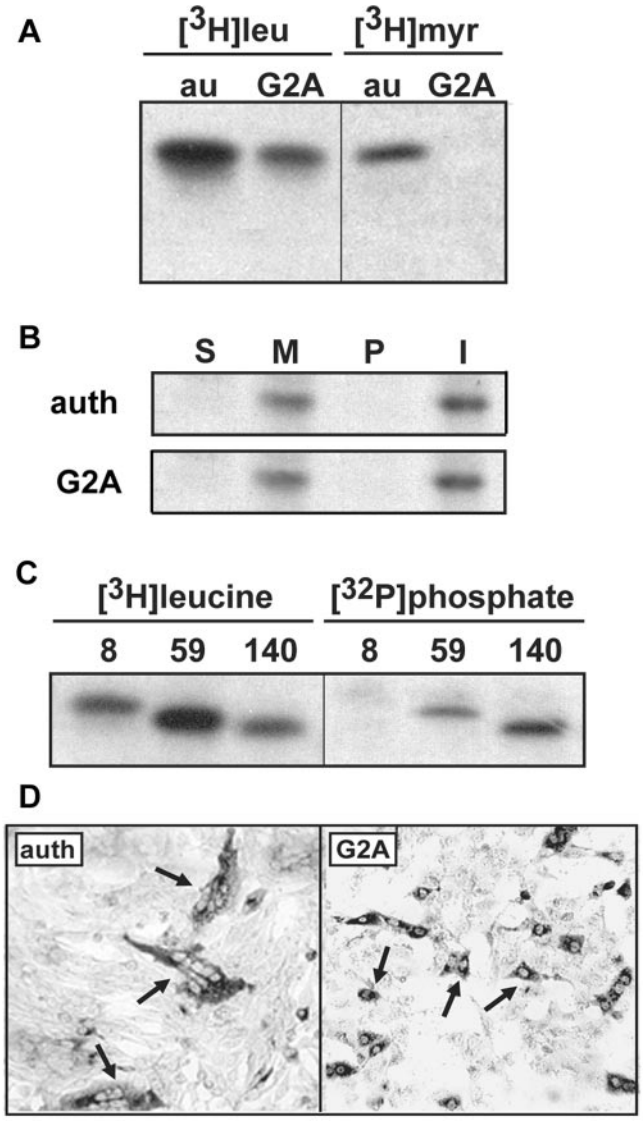

FIG. 7. N-terminal myristoylation plays an essential, nontopogenic role in p15-induced syncytium formation. (A) Cells, transfected with authentic p15 (au) or a p15 G2A construct, were labeled with [^{3}H]leucine (leu) or [^{3}H]myristate (myr), immune precipitated using anti-p15 antiserum, separated by SDS–15% PAGE, and detected by fluorography. (B) Authentic p15 (auth) or p15 G2A transcripts were translated in vitro in the presence of [^{3}H]leucine and microsomes. Translation products were separated by centrifugation into the soluble (S) and membrane-containing (M) fractions, the latter extracted with 0.5 M NaCl and recentrifuged to isolate the peripheral (P) and integral (I) membrane proteins. Samples were separated by SDS–15% PAGE and detected by fluorography. (C) Transfected cells expressing various p15 constructs containing PKA sequence tags after residue 8, 59, or 140 were labeled with either [^{3}H]leucine or with [^{32}P]phosphate in the presence of cycloheximide, immune precipitated using anti-p15 antiserum, separated by SDS–15% PAGE, and detected by fluorography. (D) Transfected cells expressing authentic p15 (auth) or p15 G2A were methanol fixed 20 h posttransfection and immunostained using rabbit anti-p15 antiserum and alkaline phosphatase-conjugated goat anti-rabbit F(ab′)$_2$. Arrows in the left panel indicate multinucleated syncytia induced by authentic p15, while in the right panel they indicate antigen-positive single-cell foci induced by the syncytium-lacking G2A construct.

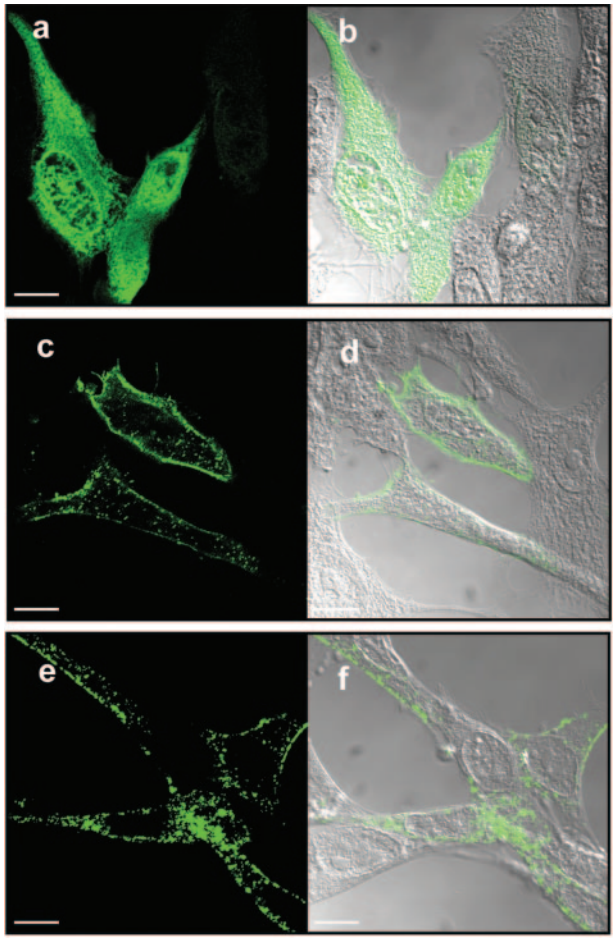

FIG. 8. N-terminal myristoylation is not required to traffick p15 to the cell surface. Transfected cells expressing GFP (a and b), p15-GFP (c and d), or p15-G2A-GFP (e and f) were methanol fixed 20 h posttransfection, following a 1 h of treatment with cycloheximide. Cell images were captured by confocal microscopy. Left panels are fluorescent images, while the right panels are an overlay of the fluorescent image and the DIC image. Scale bars, 10 μm.

and a highly basic region. We therefore propose that p15 assumes a unique bitopic membrane topology retaining both the H2 and polybasic regions in the cytosol (Fig. 9).

p15 is a type III membrane protein. The absence of a cleavable N-terminal signal peptide and the use of a signal-anchor sequence that directs translocation of a small N-terminal domain across the membrane designate p15 a type III membrane protein (23, 51). This topology classification is shared with the ARV and NBV p10 FAST proteins (45) and with the recently reported RRV p14 FAST protein (9), making a type III topology an additional defining characteristic of this unusual family of nonenveloped virus membrane fusion proteins. Typical of type III membrane proteins (13, 20, 56), the FAST proteins move relatively small (20- to 40-residue) ectodomains across the membrane.

The orientation of signal-anchor proteins in the ER membrane is dictated in large part by the charge distribution in the 15 residues that flank either side of the TM domain, with a net internal positive charge favoring an N_{exo}/C_{cyt} topology (3, 26,

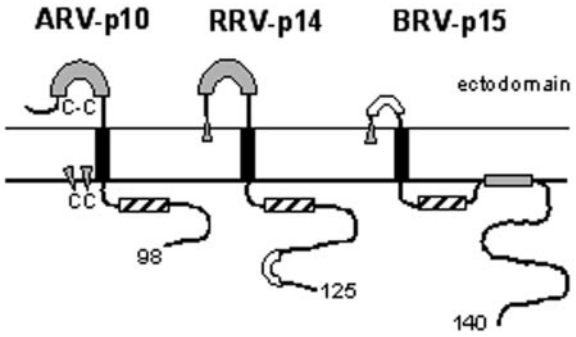

FIG. 9. Topologies of the FAST proteins, with a schematic representation of the arrangement of structural motifs in the FAST proteins. All of the FAST proteins assume bitopic N_{exo}/C_{cyt} membrane topologies, each with a single TM domain (black rectangles) and endoplasmic polybasic region (striped rectangles). Moderately hydrophobic regions (shaded rectangles) are located in the ectodomains of p10 and p14 and in the endodomain of p15. The p15 H2 hydrophobic motif is shown associated with the cytosolic leaflet of the membrane, although this has not been directly demonstrated. Open rectangles depict polyproline motifs present in the ectodomain of p15 and the endodomain of p14. The N-terminal myristate moieties in p14 and p15 (shaded triangles) are shown embedded in the outer leaflet of the membrane. The palmitate moieties present on the endodomain dicysteine motif of p10 (shaded triangles) are shown embedded in the cytosolic leaflet. A presumed intramolecular disulfide bond (C-C) between the two cysteines present in the p10 ectodomain is indicated. The arrangement of structural motifs in the ARV p10 FAST protein also applies to the NBV p10 protein. Numerals at the C terminus refer to the number of amino acid residues in each protein.

43). This situation also applies to the FAST proteins, all of which contain a membrane-proximal polybasic region in the endodomain. It is presently unclear whether the FAST protein polybasic regions serve merely as topogeneic determinants, or whether these basic regions exert other effects on the membrane fusion activity of the FAST proteins. Limited mutational analysis suggests the latter possibility. For example, insertion of acidic residues (the 18-residue double-HA tag) into the polybasic region eliminated p15 fusion activity without affecting protein topology, while insertion of additional basic residues (the 8-residue pka tag) had limited negative effects on fusion activity. Whether the different effect of these insertions was due to the nature of the residues (i.e., acidic or basic) or the relative size of the insertions is not clear. However, it is clear that alterations in the polybasic region can affect p15 fusion activity in a topology-independent manner. A similar situation exists for ARV p10 where site-specific substitutions in the polybasic region that eliminated syncytium formation did not qualitatively affect p10 membrane topology (46).

p15 contains a small, inaccessible, myristoylated ectodomain. The small size of the p15 ectodomain (approximately 20 residues), the presence of a polyproline motif that could mediate protein-protein interactions (41), and possible N-terminal-membrane interactions mediated by the externalized myristate moiety all suggest that the p15 N-terminal ectodomain may be masked by protein folding, membrane association, and/or possible protein-protein interactions. In support of this contention, antisera raised against a synthetic peptide representing the N-terminal 20 residues of p15 did not react with plasma membrane-localized p15 (data not shown). In addition, glycosylation signals created at residues 4, 9, or 17 in the p15 ectodomain were not glycosylated (S. Dawe and R. Duncan, unpublished data), while a similar glycosylation tag at residue 7 in the approximately 40-residue ectodomain of the p14 FAST protein is functional (9). It would appear that the p15 ectodomain is relatively inaccessible and/or a conformationally restricted region of the protein.

Like the RRV p14 FAST protein (9), p15 shares the unusual feature of being N-terminally myristoylated, a modification essential to the ability of both of these FAST proteins to induce membrane fusion. The p15 and p14 FAST proteins join an exceedingly rare group of integral membrane proteins that are N-myristoylated, such as cytochrome b5 (37), the hepatitis B virus large surface antigen (21, 39), and the vaccinia virus L1R protein (57). The fusion proteins of enveloped viruses are typically palmitoylated on internal, transmembrane-proximal cysteine residues (2, 6, 36, 55, 58). We know of no other examples of myristoylated viral fusion proteins, with the sole exception of the Indiana serotype of vesicular stomatitis virus that was reported to be myristoylated via a thioester bond near its C terminus (7).

The precise role of N-myristoylation in BRV p15 and RRV p14 function remains unclear. For both p14 and p15, myristoylation has limited, if any, effects on protein topology or trafficking to the plasma membrane, suggesting a more direct role in the fusion process. The myristate moiety could contribute to important reversible membrane interactions of the p15 N-terminal ectodomain with either donor or target membranes, analogous to the well-known "myristoyl-switch" mechanisms that facilitate reversible membrane interactions of cytosolic proteins (1, 25, 32, 40, 44). The protein-lipid interactions mediated by myristoylation also include those involved in protein targeting to specific membrane environments, such as raft microdomains at the cell periphery (14, 31, 42). Alternatively, myristic acid has been shown to confer localized effects on protein structure, with consequences for protein stability (29, 35, 59) or ligand binding (12, 35, 50, 54). Whatever the function, the myristate moiety in p15, like that present in p14, must exert its affect from the exoplasmic side of the lipid bilayer.

A cytosolic fusion peptide motif in p15? The hydrophobic fusion peptide motifs contained within the ectodomains of almost all virus fusion proteins play a key role in promoting lipid bilayer mixing (19, 28, 49, 53). Both the p10 and p14 FAST proteins contain modestly hydrophobic stretches in their ectodomains that are putative fusion peptides (Fig. 9) (10, 47). Such is not the case with p15, whose small ectodomain is composed mostly of polar residues and a polyproline motif. In view of its cytosolic location, the H2 region is unlikely to function as a typical fusion peptide by exerting an effect on target cell membranes. In contrast to the enveloped virus fusion proteins whose N-terminal ectodomains comprise the bulk of the polypeptide, the majority of motifs present in p15 lie proximal to the donor membrane and/or localized on the cytosolic side of the membrane. Therefore, the mechanism of p15-mediated membrane fusion may be focused on altering donor membrane interactions.

The refolding of both class I and class II enveloped virus fusion proteins ultimately results in the fusion peptide or fusion loop lying adjacent to the TM domain anchored in the

donor membrane (8, 22, 34). In addition, alternative models of enveloped virus protein-mediated membrane fusion propose that at least a proportion of the fusion peptides present in the fusion proteins aggregated at the fusion site may interact with the donor membrane, not the target membrane (4, 30). Therefore, in addition to the possible influences of the polybasic region and myristate moiety on the donor membrane discussed above, the p15 H2 region may also exert effects on donor membrane stability, functioning as a "cytosolic fusion peptide." In this regard, the size (20 residues), glycine-alanine content (30%), and relative hydrophobicity (0.59) of the H2 region are all features common to enveloped virus fusion peptides (11). Mutagenic analysis of the H2 region required to discern the role of this motif in altering donor membrane interactions, pore formation, and/or pore expansion is currently under way.

Membrane fusion with small ectodomains. In the case of enveloped viruses, fusion of the viral envelope with target cell membranes is dependent on extensive protein refolding to mediate the first two steps in the membrane fusion reaction, membrane attachment and close membrane apposition (5, 8, 27). In contrast, the nonstructural FAST proteins function more as "cellular" fusion proteins than as viral fusion proteins, mediating cell-cell fusion rather than virus-cell fusion. Consequently, p15 has the option to rely on cellular adhesion proteins to mediate close cell-cell contact. According to this model, p15 would only need to localize to regions of the plasma membrane involved in cell-cell contact and then catalyze the latter stages in the fusion reaction, lipid-mixing and pore formation. In the absence of large ectodomains, the above model also predicts that lipid mixing and pore formation may not necessarily be dependent on extensive energy input provided by structural remodeling of large, metastable ectodomains. This is in marked contrast to the majority of models for protein-mediated membrane fusion, where the energy-releasing conformational changes that mediate close membrane apposition are also required to deform the donor and/or target membrane as part of the fusion reaction (4, 5, 30, 33). Regardless of the actual mechanism, the unusual topological distribution of structural motifs in the p15 FAST protein suggests the membrane fusion reaction is likely to differ significantly from existing models of protein-mediated membrane fusion.

ACKNOWLEDGMENTS

We thank Claire Barber for contributing to the p15-calnexin coimmunofluorescence studies and Jingyun Shou for expert technical assistance.

This research was supported by grants from the Canadian Institutes of Health Research (CIHR). S.D. was funded by scholarships from the Natural Sciences and Engineering Research Council (NSERC) of Canada and the Killam Foundation. J.S. was supported by a NSERC scholarship. R.D. is the recipient of a CIHR-RPP Investigators Award.

REFERENCES

1. **Ames, J. B., R. Ishima, T. Tanaka, J. I. Gordon, L. Stryer, and M. Ikura.** 1997. Molecular mechanics of calcium-myristoyl switches. Nature **389:**198–202.
2. **Andersson, A. M., L. Melin, A. Bean, and R. F. Pettersson.** 1997. A retention signal necessary and sufficient for Golgi localization maps to the cytoplasmic tail of a *Bunyaviridae* (Uukuniemi virus) membrane glycoprotein. J. Virol. **71:**4717–4727.
3. **Beltzer, J. P., K. Fielder, C. Fuhrer, I. Geffen, C. Handschin, H. P. Wessels, and M. Spiess.** 1991. Charged residues are major determinants of the transmembrane orientation of a signal-anchor sequence. J. Biol. Chem. **266:**973–978.
4. **Bentz, J.** 2000. Membrane fusion mediated by coiled coils: a hypothesis. Biophys. J. **78:**886–900.
5. **Blumenthal, R., M. J. Clague, S. R. Durell, and R. M. Epand.** 2003. Membrane fusion. Chem. Rev. **103:**53–69.
6. **Caballero, M., J. Carabana, J. Ortego, R. Fernandez-Munoz, and M. L. Celma.** 1998. Measles virus fusion protein is palmitoylated on transmembrane-intracytoplasmic cysteine residues which participate in cell fusion. J. Virol. **72:**8198–8204.
7. **Chen, S.** 1991. Myristylation of the envelope glycoprotein of vesicular stomatitis virus. Intervirology **32:**193–197.
8. **Colman, P. M., and M. C. Lawrence.** 2003. The structural biology of type I viral membrane fusion. Nat. Rev. Mol. Cell Biol. **4:**309–319.
9. **Corcoran, J. A., and R. Duncan.** 2004. Reptilian reovirus utilizes a small type III protein with an external myristylated amino terminus to mediate cell-cell fusion. J. Virol. **78:**4342–4351.
10. **Corcoran, J. A., R. Syvitski, D. Top, R. M. Epand, R. F. Epand, D. Jakeman, and R. Duncan.** 2004. Myristoylation, a protruding loop, and structural plasticity are essential features of a nonenveloped virus fusion peptide motif. J. Biol. Chem. **279:**51386–51394.
11. **Dawe, S., and R. Duncan.** 2002. The S4 genome segment of baboon reovirus is bicistronic and encodes a novel fusion-associated small transmembrane protein. J. Virol. **76:**2131–2140.
12. **De Falco, S., M. Ruvo, A. Verdoliva, A. Scarallo, D. Raimondo, A. Raucci, and G. Fassina.** 2001. N-terminal myristylation of HBV preS1 domain enhances receptor recognition. J. Pept. Res. **57:**390–400.
13. **Denzer, A. J., C. E. Nabholz, and M. Spiess.** 1995. Transmembrane orientation of signal-anchor proteins is affected by the folding state but not the size of the N-terminal domain. EMBO J. **14:**6311–6317.
14. **Ding, L., A. Derdowski, J. J. Wang, and P. Spearman.** 2003. Independent segregation of human immunodeficiency virus type 1 Gag protein complexes and lipid rafts. J. Virol. **77:**1916–1926.
15. **Duncan, R.** 1999. Extensive sequence divergence and phylogenetic relationships between the fusogenic and nonfusogenic orthoreoviruses: a species proposal. Virology **260:**316–328.
16. **Duncan, R., and K. Sullivan.** 1998. Characterization of two avian reoviruses that exhibit strain-specific quantitative differences in their syncytium-inducing and pathogenic capabilities. Virology **250:**263–272.
17. **Duncan, R., Z. Chen, S. Walsh, and S. Wu.** 1996. Avian reovirus-induced syncytium formation is independent of infectious progeny virus production and enhances the rate, but is not essential, for virus-induced cytopathology and virus egress. Virology **224:**453–464.
18. **Duncan, R., J. A. Corcoran, J. Shou, and D. Stoltz.** 2004. Reptilian reovirus: a new fusogenic orthoreovirus species. Virology **319:**131–140.
19. **Epand, R. M.** 2003. Fusion peptides and the mechanism of viral fusion. Biochim. Biophys. Acta **1614:**116–121.
20. **Eusebio, A., T. Friedberg, and M. Spiess.** 1998. The role of the hydrophobic domain in orienting natural signal sequences within the ER membrane. Exp. Cell Res. **241:**181–185.
21. **Gallina, A., and G. Milanesi.** 1993. Trans-membrane translocation of a myristylated protein amino terminus. Biochem. Biophys. Res. Commun. **195:**637–642.
22. **Gibbons, D. L., M.-C. Vaney, A. Roussel, A. Vigouroux, B. Reilly, J. Lepault, M. Kielian, and F. A. Rey.** 2004. Conformational change and protein-protein interactions of the fusion protein of Semliki Forest virus. Nature **427:**320–325.
23. **Goder, V., and M. Spiess.** 2001. Topogenesis of membrane proteins: determinants and dynamics. FEBS Lett. **504:**87–93.
24. **Goder, V., P. Crottet, and M. Spiess.** 2000. In vivo kinetics of protein targeting to the endoplasmic reticulum determined by site-specific phosphorylation. EMBO J. **19:**6704–6712.
25. **Goldberg, J.** 1998. Structural basis for activation of ARF GTPase: mechanisms of guanine nucleotide exchange and GTP-myristoyl switching. Cell **95:**237–248.
26. **Hartmann, E., T. A. Rapoport, and H. F. Lodish.** 1989. Predicting the orientation of eukaryotic membrane-spanning proteins. Proc. Natl. Acad. Sci. USA **86:**5786–5790.
27. **Heinz, F. X., and S. L. Allison.** 2001. The machinery for flavivirus fusion with host cell membranes. Curr. Opin. Microbiol. **4:**450–455.
28. **Hsu, C. H., S. H. Wu, D. K. Chang, and C. Chen.** 2002. Structural characterizations of fusion peptide analogs of influenza virus hemagglutinin. Implication of the necessity of a helix-hinge-helix motif in fusion activity. J. Biol. Chem. **277:**22725–22733.
29. **Kennedy, M. T., H. Brockman, and F. Rusnak.** 1996. Contributions of myristoylation to calcineurin structure/function. J. Biol. Chem. **271:**26517–26521.
30. **Kozlov, M. M., and L. V. Chernomordik.** 1998. A mechanism of protein-mediated fusion: coupling between reforlding of the influenza hemagglutinin and lipid rearrangements. Biophys. J. **75:**1384–1396.
31. **Martin-Belmonte, F., J. A. Lopez-Guerrero, L. Carrasco, and M. A. Alonso.** 2000. The amino-terminal nine amino acid sequence of poliovirus capsid VP4 protein is sufficient to confer N-myristoylation and targeting to detergent-insoluble membranes. Biochemistry **39:**1083–1090.

32. **McLaughlin, S., and A. Aderem.** 1995. The myristoyl-electrostatic switch: a modulator of reversible protein-membrane interactions. Trends Biochem. Sci. **20:**272–276.
33. **Melikyan, G. B., R. M. Markosyan, H. Hemmati, M. K. Delmedico, D. M. Lambert, and F. S. Cohen.** 2000. Evidence that the transition of HIV-1 gp41 into a six-helix bundle, not the bundle configuration, induces membrane fusion. J. Cell Biol. **151:**413–423.
34. **Modis, Y., S. Ogata, D. Clements, and S. C. Harrison.** 2004. Structure of the dengue virus envelope protein after membrane fusion. Nature **427:**313–319.
35. **Olsen, H. B., and N. C. Kaarsholm.** 2000. Structural effects of protein lipidation as revealed by LysB29-myristoyl, des(B30) insulin. Biochemistry **39:**11893–11900.
36. **Olsen, K. E. P., and K. B. Andersen.** 1999. Palmitoylation of the intracytoplasmic R peptide of the transmembrane envelope protein in Moloney murine leukemia virus. J. Virol. **73:**8975–8981.
37. **Ozols, J., S. A. Carr, and P. Strittmatter.** 1984. Identification of the NH2-terminal blocking group of NADH-cytochrome b5 reductase as myristic acid and the complete amino acid sequence of the membrane-binding domain. J. Biol. Chem. **259:**13349–13354.
38. **Pelham, H. R.** 1991. Multiple targets for brefeldin A. Cell **67:**449–451.
39. **Persing, D. H., H. E. Varmus, and D. Ganem.** 1987. The preS1 protein of hepatitis B virus is acylated at its amino terminus with myristic acid. J. Virol. **61:**1672–1677.
40. **Randazzo, P. A., T. Terui, S. Sturch, H. M. Fales, A. G. Ferrige, and R. A. Kahn.** 1995. The myristoylated amino terminus of ADP-ribosylation factor 1 is a phospholipid- and GTP-sensitive switch. J. Biol. Chem. **270:**14809–14815.
41. **Reiersen, H., and A. R. Rees.** 2001. The hunchback and its neighbors: proline as an environmental modulator. Trends Biochem. Sci. **26:**679–684.
42. **Resh, M. D.** 1999. Fatty acylation of proteins: new insights into membrane targeting of myristoylated and palmitoylated proteins. Biochim. Biophys. Acta **1451:**1–16.
43. **Rosch, K., D. Naeher, V. Laird, V. Goder, and M. Spiess.** 2000. The topogenic contribution of uncharged amino acids on signal sequence orientation in the endoplasmic reticulum. J. Biol. Chem. **275:**14916–14922.
44. **Seykora, J. T., M. M. Myat, L. A. Allen, J. V. Ravetch, and A. Aderem.** 1996. Molecular determinants of the myristoyl-electrostatic switch of MARCKS. J. Biol. Chem. **271:**18797–18802.
45. **Shmulevitz, M., and R. Duncan.** 2000. A new class of fusion-associated small transmembrane (FAST) proteins encoded by the non-enveloped fusogenic reoviruses. EMBO J. **19:**902–912.
46. **Shmulevtiz, M., J. Salsman, and R. Duncan.** 2003. Palmitoylation, membrane-proximal basic residues, and transmembrane glycine residues in the reovirus p10 protein are essential for syncytium formation. J. Virol. **77:**9769–9779.
47. **Shmulevitz, M., R. F. Epand, R. M. Epand, and R. Duncan.** 2004. Structural and functional properties of an unusual internal fusion peptide in a nonenveloped virus membrane fusion protein. J. Virol. **78:**2808–2818.
48. **Skehel, J. J., and D. C. Wiley.** 2000. Receptor binding and membrane fusion in virus entry: the influenza hemagglutinin. Annu. Rev. Biochem. **69:**531–569.
49. **Skehel, J. J., K. Cross, D. Steinhauer, and D. C. Wiley.** 2001. Influenza fusion peptides. Biochem. Soc. Trans. **29:**623–626.
50. **Sowadski, J. M., C. A. Ellis, and Madhusudan.** 1996. Detergent binding to unmyristylated protein kinase A—structural implications for the role of myristate. J. Bioenerg. Biomembr. **28:**7–12.
51. **Spiess, M.** 1995. Heads or tails—what determines the orientation of proteins in the membrane. FEBS Lett. **369:**76–79.
52. **Stiasny, K., S. L. Allison, C. W. Mandl, and F. X. Heinz.** 2001. Role of metastability and acidic pH in membrane fusion by tick-borne encephalitis virus. J. Virol. **75:**7392–7398.
53. **Tamm, L. K., X. Han, Y. Li, and A. L. Lai.** 2002. Structure and function of membrane fusion peptides. Biopolymers **66:**249–260.
54. **Tholey, A., R. Pipkorn, D. Bossemeyer, V. Kinzel, and J. Reed.** 2001. Influence of myristoylation, phosphorylation, and deamidation on the structural behavior of the N-terminus of the catalytic subunit of cAMP-dependent protein kinase. Biochemistry **40:**225–231.
55. **Veit, M., E. Kretzschmar, K. Kuroda, W. Garten, M. F. Schmidt, H. D. Klenk, and R. Rott.** 1991. Site-specific mutagenesis identifies three cysteine residues in the cytoplasmic tail as acylation sites of influenza virus hemagglutinin. J. Virol. **65:**2491–2500.
56. **Wahlberg, J. M., and M. Spiess.** 1997. Multiple determinants direct the orientation of signal-anchor proteins: the topogenic role of the hydrophobic signal domain. J. Cell Biol. **137:**555–562.
57. **Wolffe, E. J., S. Vijaya, and B. Moss.** 1995. A myristylated membrane protein encoded by the vaccinia virus L1R open reading frame is the target of potent neutralizing monoclonal antibodies. Virology **211:**53–63.
58. **Yang, C., C. P. Spies, and R. W. Compans.** 1995. The human and simian immunodeficiency virus envelope glycoprotein transmembrane subunits are palmitoylated. Proc. Natl. Acad. Sci. USA **92:**9871–9875.
59. **Yonemoto, W., M. L. McGlone, and S. S. Taylor.** 1993. N-myristylation of the catalytic subunit of cAMP-dependent protein kinase conveys structural stability. J. Biol. Chem. **268:**2348–2352.